



RESEARCH ARTICLE

Using continuous electrical conductivity measurements to derive major solute concentrations in karst systems

Beatrice Richieri¹  | Daniel Bittner^{2,3} | Andreas Hartmann³ | Paolo Benettin⁴  | Boris M. van Breukelen⁵ | David Labat⁶ | Gabriele Chiogna^{1,7}

¹Chair of Hydrology and River Basin Management, TUM School of Engineering and Design, Technical University of Munich, Munich, Germany

²Department for River Basin Management, Ertfverband, Bergheim, Germany

³Institute of Groundwater Management (IGW), Technical University of Dresden, Dresden, Germany

⁴Laboratory of Ecohydrology ENAC/IIE/ECHO, École Polytechnique Fédérale de Lausanne, Lausanne, Switzerland

⁵Department of Water Management, Faculty of Civil Engineering and Geosciences, Delft University of Technology, Delft, CN, The Netherlands

⁶Géosciences Environnement Toulouse (GET), Université Toulouse 3-Géosciences Environnement Toulouse-CNRS-UPS-IRD, Toulouse, France

⁷Institute of Geography, University of Innsbruck, Innsbruck, Austria

Correspondence

Beatrice Richieri, Chair of Hydrology and River Basin Management, TUM School of Engineering and Design, Technical University of Munich, Arcisstr. 21, 80333 Munich, Germany.

Email: beatrice.richieri@gmail.com

Funding information

Deutsche Forschungsgemeinschaft; École Polytechnique Fédérale de Lausanne; European Regional Development Fund

Abstract

Hydrochemical data of karst springs provide valuable insights into the internal hydrodynamical functioning of karst systems and support model structure identification. However, the collection of high-frequency time series of major solute species is limited by analysis costs. In this study, we develop a method to retrieve the individual solute concentration time series and their uncertainty at high temporal resolution for karst springs by using continuous observations of electrical conductivity (EC) and low-frequency ionic measurements. Due to the large ion content and non-negligible concentrations of aqueous complexes in karst systems, the concentration of each solute species occurring as free ion and as part of aqueous complexes are computed separately. The concentration of species occurring as free ions are computed considering their contributions to the total EC, whereas the concentration of the species as part of complexes are obtained from speciation calculations. The pivotal role of the complexation processes for the reconstruction of solute concentration time series starting from the EC signal is investigated in two karstic catchments with different geologies and temporal resolution of the available hydrochemical datasets, that is the Kerschbaum dolostone system in Austria and the Baget limestone system in France. The results show that complexation processes are significant and should be considered for the estimation of the total solute concentration in case of SO_4 , Ca, Mg and HCO_3 . The EC signal of a karst spring can be used to interpolate and quantify the dynamics of those solutes characterized by large contribution (approximately >6%) to the total EC and low relative variability, that is HCO_3 , Ca and Mg. Moreover, the presented method can be used to estimate concentrations of solutes when applied to karst systems with stationary and hydrogeochemical homogeneous contributing area. On the contrary, the method is affected by large uncertainty in case of dynamic systems characterized by varying contributions of water from different geological areas. This study aims to contribute to the problem of hydrogeochemical data availability and to support future works on karst systems conceptualization.

This is an open access article under the terms of the [Creative Commons Attribution](https://creativecommons.org/licenses/by/4.0/) License, which permits use, distribution and reproduction in any medium, provided the original work is properly cited.

© 2023 The Authors. *Hydrological Processes* published by John Wiley & Sons Ltd.

KEYWORDS

electrical conductivity decomposition, high-resolution hydrochemical data, hydrochemical modelling, karst

1 | INTRODUCTION

The use of multiple data sources to improve our understanding of the karst hydrological functioning is getting more and more attention. For example, hydrochemical data of karst springs provide valuable insights into the internal hydrodynamical functioning, for example to characterize different kinds of karst systems or to differentiate between the contribution from the critical zone, conduit and matrix compartments under varying hydrometeorological conditions (Aquilina et al., 2006; Dreiss, 1989; Frank et al., 2019; Hartmann et al., 2013; Hartmann & Andreo, 2017; Liu et al., 2004; Mudarra & Andreo, 2011; Ravbar et al., 2011; Torresan et al., 2020). Therefore, it is important to collect and analyse hydrogeochemical information in karst systems.

Karst systems are characterized by a complex hydrologic response and rapid discharge variations that may change by one order of magnitude within hours or days (Hartmann et al., 2014). To investigate flow and transport processes in such systems, the hydrochemical sampling frequency should be comparable to the time scale of the hydrological response of the system, that is hours to days. However, high-frequency monitoring is generally restricted to continuous measurements of water level, discharge, temperature and electrical conductivity (EC), whereas the collection of high-frequency time series of major solute species for example Ca, Mg and HCO_3^- , is limited by high analysis costs (Charlier et al., 2012).

Recently, few studies investigated methods to derive continuous time series of major ions without the need of continuous measurements of these ions. Mewes et al. (2020) tested the ability of different machine learning algorithms to interpolate time series of natural tracer concentrations in karstic environment and to predict SO_4^{2-} and NO_3^- concentrations from discharge data. While the study showed that machine learning algorithms are valuable to fill gaps between point measurements of ionic concentrations, these algorithms cannot predict the tracers' temporal variability (Mewes et al., 2020).

Benettin and van Breukelen (2017) proposed a method to derive the individual ion concentration from the total ion content information embedded in the EC signal measured at a river gauge. The approach is based on the decomposition of the EC into the specific contributions of the major free ions that conduct electrical current in water. EC can be easily and cheaply measured by means of automatic instruments and thus shows a huge potential in model development and evaluation (Cano-Paoli et al., 2019; Chang et al., 2021; Hayashi et al., 2012; Jourde et al., 2018; Meus et al., 2014). Starting from continuous EC data and ionic point measurements, the method of Benettin and van Breukelen (2017) makes it possible to estimate ionic concentration time series at the same temporal resolution as the EC signal. The approach was tested on data from the Upper Hafren river catchment in the Plynlimon area, mid-Wales, United Kingdom, characterized by low EC values (average of 29 $\mu\text{S}/\text{cm}$) and by a total ion content dominated by Cl and Na, which have no or little tendency to be involved in

complexation processes. The approach proved to give a better representation of the ion dynamics than a direct linear interpolation of the concentration point measurements. Similar approaches were used to first establish regressions between ionic concentrations and laboratory measurements of EC and then to decompose the EC measured at river gauges into the major ion contributions (Lechuga-Crespo et al., 2020).

Differently from the Upper Hafren river catchment, karstic environments can be characterized by large content of solutes that could form complexes and EC values around 500 $\mu\text{S}/\text{cm}$ (Chang et al., 2021; Hilberg & Schneider, 2011; Sheikhy Narany et al., 2019). The large ion content and the complex hydrogeochemical interactions between water and the matrix cause the discharge of a karst spring to often show an intricate water speciation. Due to the non-negligible concentrations of aqueous complexes in karst systems, there is the necessity to modify the methodology proposed by Benettin and Van Breukelen (2017) to account for aqueous complexation processes. The aim of the present work is hence to develop a method to retrieve individual solute species concentration time series at high resolution from continuous EC measurements in karst springs, by explicitly accounting for complexation processes. Indeed, some solute species, like SO_4 , Ca and HCO_3 , have high tendency to form complexes, which thus need to be considered in the reconstruction of the total concentration, despite not having a significant influence on the total EC of the water. Moreover, we investigate the uncertainties related to the quantification of each individual solute species both for interpolation and prediction of high-resolution concentration time series. Since different geological structures and rock types of a system determine the flow regime and aqueous chemistry (Odeh et al., 2009), we consider two karstic watersheds with different types of bedrock and temporal resolution of the available hydrochemical datasets, that is the Kerschbaum dolostone system in Austria (quarterly, weekly and 5-h sampling temporal resolutions) and the Baget limestone system in France (sampling temporal resolution from 1 to 4 h). Thus, by testing the approach on karst systems characterized by different geology and different sampling frequency, we evaluate the relevance of complexation processes in karst systems characterized by different degrees of complexity.

2 | MATERIALS AND METHODS

2.1 | Study areas

We consider two study areas, that is the Kerschbaum dolostone karst system in Austria and the Baget limestone karst system in France (Figure 1a). The different geological formations characterizing the two spring watersheds (Figure 1b,c) result in different degree of karstification, discharge variability and solute transport processes.

The Kerschbaum spring is located 10 km south of the city of Waidhofen a.d. Ybbs, Austria (Figure 1a,b). The pre-alpine springshed

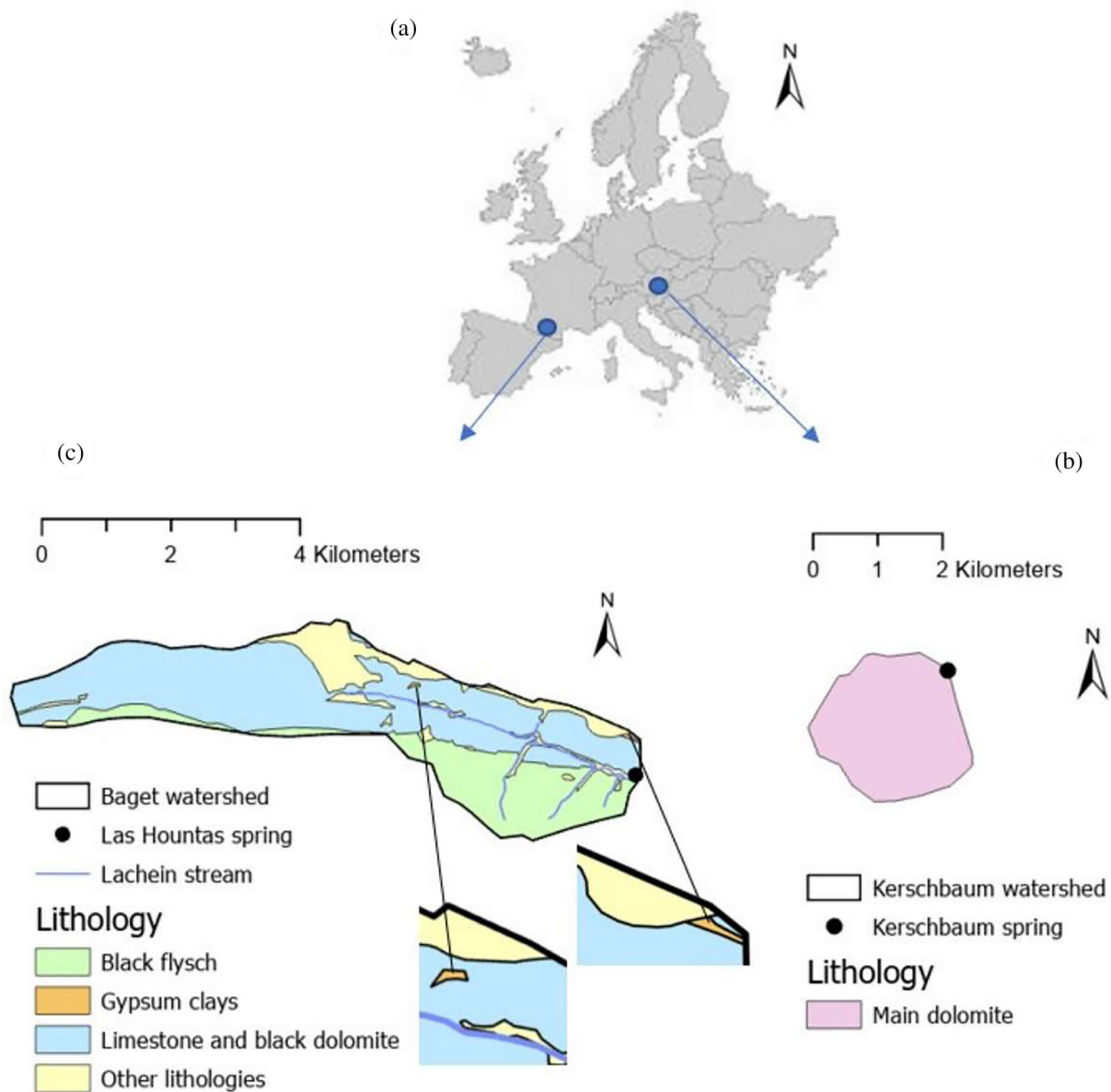


FIGURE 1 Geological maps of the study areas showing the location of the springs and recharge areas. a The locations of the study areas in Europe. b Kerschbaum dolostone karst system in Austria. c Baget limestone karst system in France.

covers approximately 2.5 km² and is part of the eastern foothills of the Northern Calcareous Alps, showing a homogeneous dolomitic geology. The Kerschbaum spring aquifer is characterized by a complex small-scale groundwater karst system with a deep and developed network of fractures and conduits (Hacker, 2003; Sheikhy Narany et al., 2019). Despite the dominance of carbonate bedrocks, the study area does not show significant sinkholes. Therefore, we assume that point infiltration and concentrated recharge processes scarcely contribute to the groundwater recharge and, thus, that the spring discharge is controlled by diffusive infiltration. Consequently, the response of the spring discharge to precipitation events is characterized by a piston and flushing effect of the dissolved elements stored in the saturated zone. The recharge area is primarily covered with forests and is characterized by a mean annual temperature of 8°C and mean annual precipitation of 1379 mm (period from 1981 to 2014). The annual rainfall distribution

is bimodal with a peak in the summer (June and July) and a peak in the winter (December and January) (Bittner et al., 2018). The Kerschbaum spring is an important source of fresh water providing a mean discharge of 34 L/s to the regional water supply and shows a fast reaction time to precipitation events of 1 day (Bittner et al., 2021).

The Baget karst system (13 km²) is located in the Pyrenees, in the Ariège administrative department (Figure 1a-c). The main perennial spring of the Baget catchment, called Las Hountas, is mainly recharged by the calcareous formation of the Jurassic and Lower Cretaceous, with a mineralogical composition dominated by calcite. Despite the large occurrence of limestone bedrocks, the catchment is also characterized by an outcrop impermeable formation of black flysch, which strongly influences the hydrochemical composition of the spring discharge due to pyrite oxidation and consequent formation of strong acids, that is sulfuric acid. Minor gypsum and dolomitic rocks are also observed in the

watershed. The different geologies present in the area affect the temporal variability of the spring discharge displaying a complex response characterized by different mechanisms, that is dilution processes during high discharge periods, piston and flushing effects after long dry periods and varying contributions of water draining different areas of the watershed (Ulloa-Cedamano et al., 2020). The water from calcareous formations feeds the subsurface karst system through seepage or water losses of the Lachein stream, which is usually dry and gets activated only at high flow conditions. Las Hountas is the only perennial spring of the Baget catchment and it is representative of a part of the total response of the karstic watershed. Indeed, during high flood events, when the upper part of the catchment is active, there is water bypassing the spring (Mangin, 1975; Ulloa-Cedamano et al., 2021). The Baget catchment is mainly covered by fir-beech forest and is under the influence of the Atlantic oceanic climate with an annual air temperature of 12.3°C and an average annual rainfall close to 1700 mm. The annual rainfall distribution is bimodal with a first peak in December and a second one in February. The average annual discharge is 477 L/s with no influence of snow melt processes (Ulloa-Cedamano et al., 2020).

2.2 | Datasets

Tables 1 and 2 show the temporal resolution, number of samples and the statistics of the measured EC ($\mu\text{S}/\text{cm}$) and major solute species of

interest, that is Ca, Mg, HCO_3 , SO_4 , NO_3 , Cl, Na and K (mg/L), for both the studied areas and available data periods.

The EC was measured in the field at the Kerschbaum spring using a conductivity meter (HT Hydrotechnik, Typ 575-LTC) and reported at 25°C. During data preprocessing, the EC signal in 2018–2019 was corrected to compensate for an offset of the probe of 19 $\mu\text{S}/\text{cm}$. The solute concentration measurements were provided by the waterworks of Waidhofen a.d. Ybbs for the periods 2000–2016 and 2018–2019 at different temporal resolutions. During the period from 23 January 2022 to 28 January 2022, water samples were collected every 5 h by means of a 6712 ISCO sampler.

The EC at the perennial spring Las Hountas was measured continuously with a temporal resolution of 15 min using an In-Situ Aqua TROLL 200 device. To collect water samples for ionic measurements, a 6712 ISCO sampler was installed at the spring and connected to the EC probe. To enable an efficient sampling at the spring during storm conditions, the sampler was programmed to automatically start sampling above a given water level threshold (30 cm). In total, three precipitation events were gauged, the first from 4 October 2021 to 14 October 2021, the second from 1 November 2021 to 7 November 2021 and the third from 20 November 2022 to 26 November 2022. For all the events, the temporal resolution of the sampling was 1 h during the rising limb of the hydrograph, while it was set to 2 h during the recession phase. To record the baseflow following the end of each precipitation event, we collected composite samples, integrating 8 h

TABLE 1 Summary of the datasets characteristics, including: temporal resolution (TR), number of samples (n), mean, standard deviation (sd), minimum (Min) and maximum (Max) values of the electrical conductivity EC ($\mu\text{S}/\text{cm}$) and major solute species (mg/L) measured at the Kerschbaum spring for the periods 2000–2016, 2018–2019, and 23 January 2022–28 January 2022.

	EC ($\mu\text{S}/\text{cm}$)	Ca (mg/L)	Mg (mg/L)	HCO_3 (mg/L)	SO_4 (mg/L)	NO_3 (mg/L)	Cl (mg/L)	Na (mg/L)	K (mg/L)
<i>Kerschbaum spring 2000–2016</i>									
TR	Quarterly	Quarterly	Quarterly	Quarterly	Quarterly	Quarterly	Quarterly	Quarterly	Quarterly
n	64	62	62	62	62	62	62	62	62
Mean	474.4	58.8	26.6	294.8	8.2	5.4	6.3	3.5	0.7
SD	20.9	3.5	1.2	10.9	1.3	0.4	3.2	1.1	0.1
Min	430	49	24.7	230.7	5.8	4	3	1.9	0
Max	550	74	31	322	11	6.6	23.3	9.5	0.9
<i>Kerschbaum spring 2018–2019</i>									
TR	Hourly	Weekly	Weekly	Weekly	Weekly	Weekly	Weekly	Weekly	Weekly
n	8423	41	41	41	41	41	41	41	41
Mean	481	60.1	26.3	297.9	6.1	5.5	5.9	3.6	0.1
SD	11.9	1.8	0.7	3.5	0.7	0.3	1.4	0.7	0.3
Min	468	56.3	24.9	292.3	5.1	4.8	4.6	2.8	0
Max	565	64.9	27.6	307.1	7.6	6	11.7	5.8	1.1
<i>Kerschbaum spring 23/1/2022–28/1/2022</i>									
TR	Quarte- hour	5-h	5-h	5-h	5-h	5-h	5-h	5-h	5-h
n	461	24	24	24	24	24	24	24	24
Mean	506.8	67.9	28.2	319.3	8.4	7	9.6	4.7	1.1
SD	1.9	1.4	0.7	2.9	0.03	0.1	0.5	0.1	0.1
Min	503.4	65.2	27	317.3	8.3	6.8	8.6	4.3	0.9
Max	509.6	70.5	29.5	323.4	8.4	7.2	10	4.9	1.3

TABLE 2 Summary of the datasets characteristics, including: temporal resolution (TR), number of samples (n), mean, standard deviation (sd), minimum (Min) and maximum (Max) values of the electrical conductivity EC ($\mu\text{S}/\text{cm}$) and major solute species (mg/L) measured at the Las Hountas spring for the events 4/10/2021–14/10/2021, 1/11/2021–7/11/2021, and 20/11/2022–26/11/2022.

	EC ($\mu\text{S}/\text{cm}$)	Ca (mg/L)	Mg (mg/L)	HCO ₃ (mg/L)	SO ₄ (mg/L)	NO ₃ (mg/L)	Cl (mg/L)	Na (mg/L)	K (mg/L)
<i>Las Hountas spring 4/10/2021–14/10/2021</i>									
TR	quarte hour	event based	event based	event based	event based	event based	event based	event based	event based
n	1005	65	65	65	65	65	65	65	65
Mean	340.6	60.2	5.6	192.4	16.5	3.3	1.4	1	0.4
SD	15	2.5	0.3	5.6	6.3	0.1	0.1	0.06	0.1
Min	316	54.1	5.1	182.4	10.9	3.1	1.3	0.9	0.3
Max	401.3	67.9	6.7	201.4	42.5	3.8	1.9	1.3	0.9
<i>Las Hountas spring 1/11/2021–7/11/2021</i>									
TR	quarte hour	event based	event based	event based	event based	event based	event based	event based	event based
n	633	77	77	77	77	77	77	77	77
Mean	355.9	70	5.4	210.4	22.1	3.8	2.3	1.1	1.3
SD	16.4	3.8	0.2	6.4	5.5	0.2	0.2	0.1	0.4
Min	328	63.6	5.1	189.2	15	3.6	2.2	1	0.5
Max	410	77	6.1	219.7	42	4.2	2.4	1.3	1.9
<i>Las Hountas spring 20/11/2022–26/11/2022</i>									
TR	quarte hour	event based	event based	event based	event based	event based	event based	event based	event based
n	619	103	103	103	103	103	103	103	103
Mean	352.2	62.2	5.5	198.4	21.2	5.1	1.8	1.1	0.5
SD	15.1	3.1	0.5	9.1	11	1.7	0.3	0.1	0.1
Min	319.	55.7	4.4	185.6	6.8	2.4	1.4	0.9	0.3
Max	418.7	70.8	7.1	230.5	50.8	8.9	2.7	1.5	1

samples each. All the collected samples were analysed in terms of major solute concentrations.

The specifications of the laboratory analysis for the datasets of Kerschbaum and Las Hountas are reported in the Supplementary Materials S1 and S2, respectively. During the preprocessing of the data of both the study areas, the charge balance of each sample was checked using the software PHREEQC (Parkhurst & Appelo, 2013) and the samples with an error larger than $\pm 5\%$ are considered too uncertain and eliminated from the datasets.

2.3 | EC decomposition method

Our methodology aims to retrieve individual solute species concentrations at high temporal resolution for the specific case of karst springs starting from the work of Benettin and van Breukelen (2017), which we modify to consider complexation processes in the karstic environments of the springs. The observed EC signal is decomposed into the major solute species concentrations at the same temporal resolution as the available EC data, based on the results of ionic measurements of water samples collected at lower temporal resolution than EC. Due to sample preparation procedures, the total concentration of a solute species measured in the laboratory consists of the sum of that species as free ion and as part of aqueous complexes. The concentrations of each species occurring as free ions and as complexes are first computed separately, then summed together and compared to the total

solute species concentrations obtained with laboratory analyses. The concentrations of the species present as free ions are computed based on the contributions of each ion to the total measured EC, whereas the concentrations of the species involved in complexes are derived with speciation calculations. The workflow is as follows:

1. Estimation of the contribution of each free ion to the total EC: The EC is a measure of the water's capability to pass an electrical flow through the movement of charged ions and results from the total amount of dissolved solid (Massei et al., 2007). Consequently, the total EC ($\mu\text{S}/\text{cm}$) of water can be expressed as the sum of the contributions of each individual ionic species i (Equation 1).

$$EC = \sum_i EC_i \tag{1}$$

The contribution of the species i to the total electrical conductivity (EC_i) is computed from Equations (2S)–(5S) presented in the Supplementary Material S3. As suggested by Benettin and van Breukelen (2017), the chemical properties of each ion i can be grouped in a single coefficient a_i ($(\mu\text{S}/\text{cm})/(\text{mg}/\text{L})$) as:

$$a_i = \frac{\Lambda_m^\circ * \gamma_{EC}}{M} \tag{2}$$

with Λ_m° the molar conductivity ($\mu\text{S m}^2/\text{mol}$), γ_{EC} the electrochemical activity coefficient (-) and M the solute molar mass (g/mol) of the individual ion.

Equations (1S)–(6S), which are reported in Supplementary Material S3, can be implemented on PHREEQC to derive the EC_i of the free ions Ca^{2+} , Mg^{2+} , HCO_3^- , SO_4^{2-} , NO_3^- , Cl^- , Na^+ and K^+ . The PHREEQC file containing the implemented equations to compute the EC_i and a_i of each ion is reported in the Supplementary Material S4. In addition, for a more detailed explanation of the procedure, one can refer to the PHREEQC manual (Parkhurst & Appelo, 2013).

Following the approach of Benettin and van Breukelen (2017), for each free ion i is possible to define a ‘weight factor’ $f_{i(-)}$ that describes how much the free ion contributes to the total EC based on its chemical properties and concentration:

$$f_i(t) = \frac{EC_i(t)}{EC(t)} = \frac{a_i(t) \times C_i(t)}{EC(t)} \quad (3)$$

The weights f_i can only be measured at times t , when the ion concentration $C_i(t)$ is available.

- Linear interpolation of the weights f_i to obtain high-resolution major free ion time series: The low-frequency weight factors f_i (Equation 3) are linearly interpolated to the same high-resolution time scale of the observed EC. Then, the high-frequency concentrations C_i time series of the individual solute species as free ions are computed with the inverse of Equation (3).

$$C_i(t) = \frac{EC(t) * f_i(t)}{a_i(t)} \quad (4)$$

- Computation of high-resolution time series of species involved in aqueous complexes: The concentrations of the species involved in complexes cannot be derived by applying the same method used for the species as free ions. Some complexes, such as $NaSO_4^-$ and $CaHSO_4^+$, involve more than one of the species of interest, that is Ca, Mg, HCO_3 , SO_4 , NO_3 , Cl and Na. Thus, it is not possible to directly correlate the contribution of a complex to the total observed EC and the concentrations of the individual species. In addition, even if this correlation was possible, the low contribution of the complexes to the total measured EC would result in large errors in the computed concentrations. Indeed, Benettin and van Breukelen (2017) found out that species with small contribution to the total EC are prone to high relative errors on the estimation of the weight factors f_i and thus more difficult to isolate in the EC decomposition. Instead, the concentration of each individual species, which would form complexes under the given conditions, is derived at the resolution of the collected water samples by speciation calculations with PHREEQC as difference between the total molality of a species (mol/kgw) and the molality of the solution (mol/kgw). The PHREEQC file containing the implemented equations is reported in the Supplementary Material S4. The derived low-resolution concentrations of each complex are then linearly interpolated at the temporal resolution of the measured EC.

- Finally, the total concentration time series at high resolution of each major solute species of interest, that is Ca, Mg, HCO_3 , SO_4 ,

NO_3 , Cl, Na and K, is computed as the sum of the concentrations of that species as free ion and as involved in complexes.

2.4 | Uncertainty quantification

In the present study, we investigate both the uncertainty on the individual solute concentrations resulting from the experimental error on f_i , and the uncertainty derived by considering f_i as random variables (Section 2.4.1). Moreover, we propose to use the described methodology not only to interpolate between the coarse samples, but also to reconstruct the ion content for periods in which only the EC data are available (Section 2.4.2). The presented analyses are done for both the Kerschbaum and Las Houtas. However, since for the Kerschbaum spring no ionic measurements were available at peak spring discharge conditions in January 2019, the results of the uncertainty quantification for Kerschbaum are reported in the Supplementary Material.

2.4.1 | Uncertainty quantification of the weight factors f_i

Each value of $f_i(t)$ is affected by uncertainty that propagates from the $EC(t)$ measurement error and from the error in the ion concentration obtained at the coarse temporal scale as shown in Equation (3). We can then quantify the uncertainty $\delta f_i(t)$ on the weight factor $f_i(t)$, assuming that the uncertainty affecting $a_i(t)$ is negligible, according to (Fornasini, 2008):

$$\delta f_i(t) \simeq \sqrt{\left[\left(\frac{\delta f_i(t)}{\delta EC(t)} \right)_0^2 \times (\delta EC(t))^2 + \left(\frac{\delta f_i(t)}{\delta C_i(t)} \right)_0^2 \times (\delta C_i(t))^2 \right] \times a_i(t)^2} \quad (5)$$

which results in:

$$\begin{aligned} (\delta f_i(t))^2 &\simeq \left[\left(\frac{\delta f_i(t)}{\delta EC(t)} \right)_0^2 * (\delta EC(t))^2 + \left(\frac{\delta f_i(t)}{\delta C_i(t)} \right)_0^2 * (\delta C_i(t))^2 \right] \times a_i(t) = \\ &= \left[\frac{1}{C_{i0}(t)^2} * (\delta EC(t))^2 + \frac{EC_0(t)^2}{C_{i0}(t)^4} * (\delta C_i(t))^2 \right] \times a_i(t) \end{aligned} \quad (6)$$

$$\left(\frac{\delta f_i(t)}{f_{i0}(t)} \right)^2 \simeq \left[\left(\frac{\delta EC(t)}{EC_0(t)} \right)^2 + \left(\frac{\delta EC(t)}{C_{i0}(t)} \right)^2 \right] \times a_i(t) \quad (7)$$

As shown in Equation (7), we can further observe that the relative error in the weight factor f_i is always larger than the relative error in EC and C_i . Table 3 shows the values of δEC and δC_i which we consider for the analysis, their measurement device/analysis and the reference used for the estimated measurement error.

Finally, we derive the experimental uncertainty on individual solute species concentrations by applying the EC decomposition method

TABLE 3 Measurement errors used to quantify the uncertainty on the weight factor f_i , together with their value, measurement device/analysis and reference.

Measurement error	Value	Device/analysis	Reference
δEC	0.5% of reading +1 $\mu S/cm$	Aqua TROLL 200	In-Situ Inc. (2012)
$\delta C_{Ca^{2+}}$	1.22 mg/L	ICP-OES ^a	Report analysis GET ^b
$\delta C_{Mg^{2+}}$	0.08 mg/L	ICP-OES	Report analysis GET
$\delta C_{HCO_3^-}$	3 mg/L	Titration	Somridhivej and Boyd (2016)
$\delta C_{SO_4^{2-}}$	1.47 mg/L	Ion chromatography	Pfaff (1993)
$\delta C_{NO_3^-}$	0.36 mg/L	Ion chromatography	Pfaff (1993)
δC_{Cl^-}	0.29 mg/L	Ion chromatography	Pfaff (1993)
δC_{Na^+}	0.02 mg/L	ICP-OES	Report analysis GET
δC_{K^+}	0.01 mg/L	ICP-OES	Report analysis GET

^aLaboratoire Goscience Environment Toulouse.

^bInductively coupled plasma optical emission spectrometry.

considering the measured weight factors f_i and their experimental error. In addition, the experimental uncertainty on the individual species concentrations is compared with the concentration's estimates obtained considering the weight factors f_i as random variables.

2.4.2 | Predictive model based on the frequency of occurrence of the weight factors f_i

The ability of the method to determine high-resolution concentration time series of major solute species is investigated by computing the frequency of occurrence of the weight factors and applying them in a predictive manner. For Kerschbaum, the years 2000–2016 are used as period in which we estimate the frequency of occurrence of the weight factors (calibration period), while the year 2018–2019 and the event 23 January 2022–28 January 2022 are used as validation periods; for Las Hountas, the first event in October 2021 is used as calibration period, the second event in November 2021 and the third event in November 2022 as validation periods. In the calibration step, the weight factors f_i are calculated by considering the solute concentrations and total EC both measured in the calibration period (Equations 1S–6S and 3). Then, in the validation step, to predict the concentration of each solute species as free ion (Equation 4), the empirical frequency distribution of the weight factor of each free ion computed for the calibration period is combined with the total EC observed in the validation periods and a_i . The concentration of each species involved in complexes is first computed for the calibration period as described in Section 2.3 and then for the validation periods by assuming the same proportion between solutes as free ions and involved in complexes as observed in the calibration period. This assumption is done based on speciation calculations with PHREEQC, which show that the percentages of solutes as free ions and as part of complexes are constant, for each karstic spring, over the studied periods (Figure 2a–c). This analysis evaluates the

performance of the method to estimate, based on historical data, high-resolution concentrations time series when only EC observations are available.

2.5 | Investigation of different water contributions

For the case of Las Hountas, we tested different approaches to investigate the water contributions from the different geological areas present in the Baget catchment (Figure 1c).

The dissolution processes and stoichiometric relationships characterizing the calcareous rocks and black flysch are shown in the Supplementary Material S5 (Figure S1). The sulfuric acid, which comes from the black flysch, results in an alkalinity lower than what we would have in case of only carbonate dissolution by carbonic acid. The percentage decrease in alkalinity can be estimated as shown in the following equation:

$$\Delta_{Alk}(\%) = \frac{(Ca^{2+} + Mg^{2+}) - HCO_3^-}{(Ca^{2+} + Mg^{2+})} \quad (8)$$

where the ion concentrations are expressed in meq/L (Ulloa-Cedamano et al., 2020).

The computed alkalinity reduction is then correlated with the equivalent ratio SO_4^{2-} over HCO_3^- and with the performance of the method both when interpolating and predicting solute concentrations at high resolution.

In addition, the variation over time of the relative contributions to the total EC provides insights into the system functioning. More precisely, the correlation between EC, water level and weight factors of HCO_3^- and SO_4^{2-} makes it possible to investigate the water contributions from the calcareous rocks and black flysch under different discharge conditions.

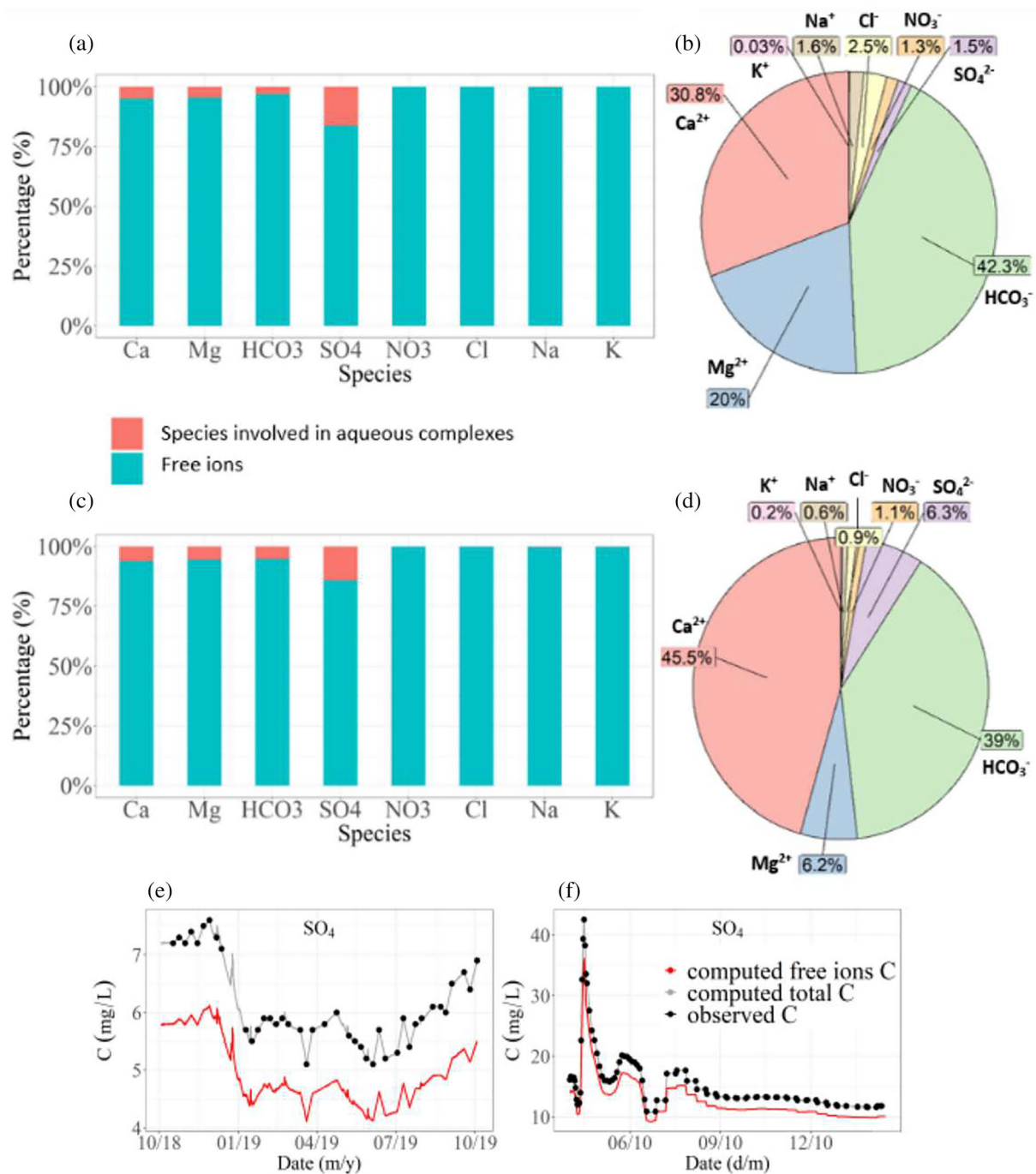


FIGURE 2 Speciation of the spring discharge. a, c Solute species occurring as free ions (%) and as involved in aqueous complexes (%) expressed, for each species, as mean percentage of the total solute concentration, together with their percentage contribution to the total electrical conductivity EC, for the Kerschbaum spring (a) and for the Las Houtas spring (c). b, d Mean contribution to the total EC (%) of each free ion observed at the Kerschbaum spring (b) and at the Las Houtas spring (d). e, f Computed total concentration, computed concentration as free ion and observed concentration of SO₄, for the Kerschbaum spring (e) and for the Las Houtas spring (f).

3 | RESULTS

3.1 | Speciation and total electrical conductivity calculations on PHREEQC

From the major solute concentrations, speciation calculations with PHREEQC provide the distribution of the aqueous species in each

water sample. Figure 2a–c shows the average percentages of each solute species as free ion and as involved in aqueous complexes for both the Kerschbaum and Las Houtas springs. The results are consistent between the two studied areas. Among the investigated solutes, SO₄ is the one with the largest tendency to form complexes, with 16.3% (Kerschbaum) and 14.2% (Las Houtas) of its total concentration involved in the formation of CaHSO₄⁺, NaSO₄⁻ and HSO₄⁻. Also,

Ca, Mg and HCO_3^- are involved in complexes (CaOH^+ , CaHSO_4^+ , CaHCO_3^+ , MgHCO_3^+ and MgOH^+) and for Kerschbaum the percentages of Ca, Mg and HCO_3^- are 5%, 4.5% and 3%, respectively, whereas for Las Hountas 6.1%, 5.5% and 5.2%, respectively. For both springs, only 0.2% of Na forms NaSO_4^- and NaCO_3^- , while NO_3^- and Cl are present only as free ions. Finally, K occurs in Kerschbaum only as free ions, whereas in Las Hountas 0.1% of it forms complexes. For the case of SO_4^{2-} , Figure 2e,f compares the computed free ion and total concentration time series and thus show the pivotal role of complexes when reconstructing the total solute concentration from the total EC.

As described in Section 2.3, the total EC is computed as the sum of the electrical conductivities EC_i of the charged individual solutes (Equations 1S–5S in the Supplementary Material). The individual free ions contribute to the total computed EC differently in the two studied areas (Figure 2b–d), due to the different geological formations of the watersheds. For the Kerschbaum spring, the contributions of HCO_3^- , Ca^{2+} and Mg^{2+} to the total EC are on average 42.1%, 30.5% and 20.1%, respectively, with about 92.7% of the total EC correlated to the dissolution of dolomite rocks. SO_4^{2-} , NO_3^- contributes with a percentage of 1.5% and 1.3%, respectively, and the total contribution of Cl^- , Na^+ and K^+ is approximately 4.1%. On the contrary, for Las Hountas, the dominance of limestone bedrocks leads to a larger contribution of Ca^{2+} (45.5%) and a lower contribution of Mg^{2+} (6.2%), while the contribution of HCO_3^- (39%) is comparable. Moreover, the black flysch formation releases SO_4^{2-} , which contributes with a percentage of 6.3% to the total EC. Finally, the total contribution of NO_3^- , Cl^- , Na^+ and K^+ is equal to 2.8%.

Figures 3a,b and 3e,f presents the EC and charge balance errors (%), respectively, computed by PHREEQC at the same temporal resolution as the measured water samples for the Kerschbaum (period 2018–2019) and Las Hountas (event 4 October 2021–14 October 2021) springs. The low frequency computed EC (dashed line) and the continuous observed EC (solid line) are plotted together in Figure 3a,b. For the case of Kerschbaum, the computed EC does not fully capture the dynamic of the system due to the low temporal resolution. For example, in December 2018 and January 2019 no water samples were collected and hence the manual sampling does not cover the period with the highest EC values. Considering the Las Hountas dataset with a higher temporal resolution of hydrochemical measurements, the computed EC time series better matches the short dynamic of the system.

The relative error time series $\left(\frac{\text{EC}_{\text{observed}} - \text{EC}_{\text{PHREEQC}}}{\text{EC}_{\text{observed}}}\right)$ and relative error probability distributions are shown in Figure 3c,d and Figure 3g,h, respectively. For Kerschbaum, the computed EC slightly underestimates the observations, with a relative error range between -0.01 and 0.05 and relative error mean of 0.02 . Las Hountas shows computed EC slightly lower than the observations. The relative error ranges from 0.01% to 0.06% and has a mean value of 0.03% . Overall, for both springs, the EC computed through Equations (1S)–(5S) by PHREEQC is satisfactory.

Finally, Figure 3e,f presents the charge error (%) time series computed for each input water sample by means of built-in functions on PHREEQC. For Kerschbaum, the charge error ranges from -1.7% to

3.7% with a mean value of 0.5% , while, for Las Hountas, it ranges between -2.8% and -0.1% with mean value of -1.2% . For both the springs, the charge error indicates an overall respected charge balance.

3.2 | Frequency of occurrence of the weight factors f_i

Figure 4 shows the violin plots comparing the frequency of occurrence and boxplots of the weight factors f_i of each major free ion observed during the available data periods. Thus, we compared the f_i observed in 2000–2016, 2018–2019 and 23 January 2022–28 January 2022 for Kerschbaum and those observed during the events in October 2021, November 2021 and November 2022 for Las Hountas. Figure 4 shows that, despite referring to events close in time, the differences between the frequency of occurrence of the weight factors f_i observed in Las Hountas are more pronounced than those observed for Kerschbaum. For Las Hountas, two events separated by a longer time interval, like the ones in October 2021 and November 2022, can display more similar distributions of the weight factors of some ions than two events closer in time (October 2021 and November 2021).

3.3 | Uncertainty quantification of the individual solute species concentrations in case of interpolation

This subsection presents the uncertainty on the individual solute species concentrations resulting from the experimental error on f_i (Equation 7), as well as the uncertainty derived by considering f_i as random variables when we apply the methodology for interpolation. Both the computed uncertainties are shown for each solute species in Figure 5 for Las Hountas (4 October 2021–14 October 2021) together with the low-resolution observed solute concentrations (red points).

The error in the interpolated solute concentrations caused by the experimental error in the estimation of f_i is shown for Las Hountas in Figure 5 and for Kerschbaum in Figures S2a and S3a with dashed red lines. We can observe that the larger the concentration of a specific solute species the lower the related experimental error on f_i and consequently on the interpolated C_i . For instance, the concentration of Mg is much larger in Kerschbaum (Table 1) than in Las Hountas (Table 2) and consequently the error in the interpolated Mg values for Las Hountas (Figure 5) is larger than for Kerschbaum (Figures S2a and S3a). On the contrary, Las Hountas shows a larger concentration of SO_4 and thus a lower experimental error than Kerschbaum.

Figure 5 also shows the uncertainty bands computed for Las Hountas considering f_i a random variable whose value is sampled from the frequency of occurrence shown in Figure 4. The measured solute concentrations are indicated with red points and, for each solute species, fall within the full-range uncertainty band. The majority of the observed concentrations are included in the computed

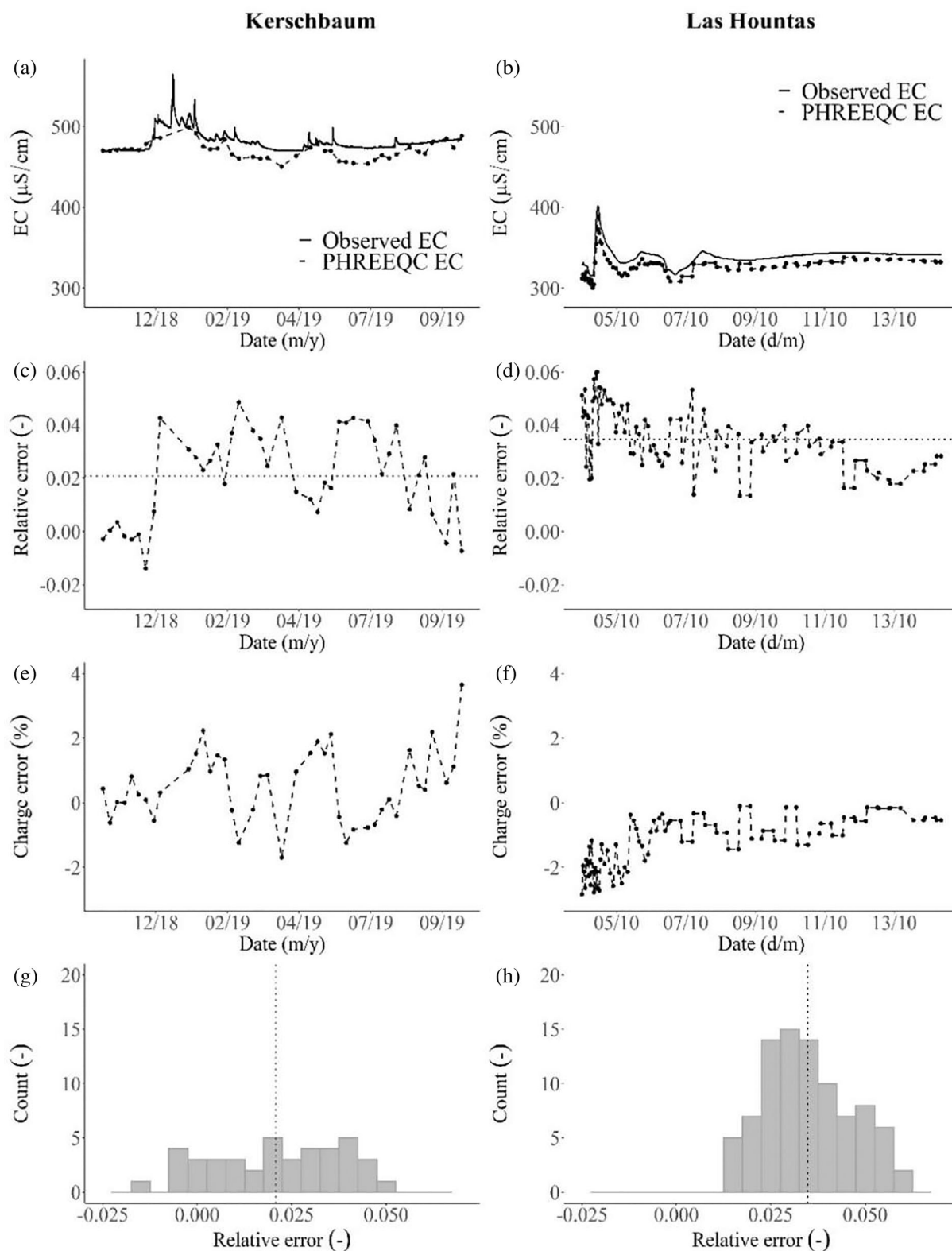
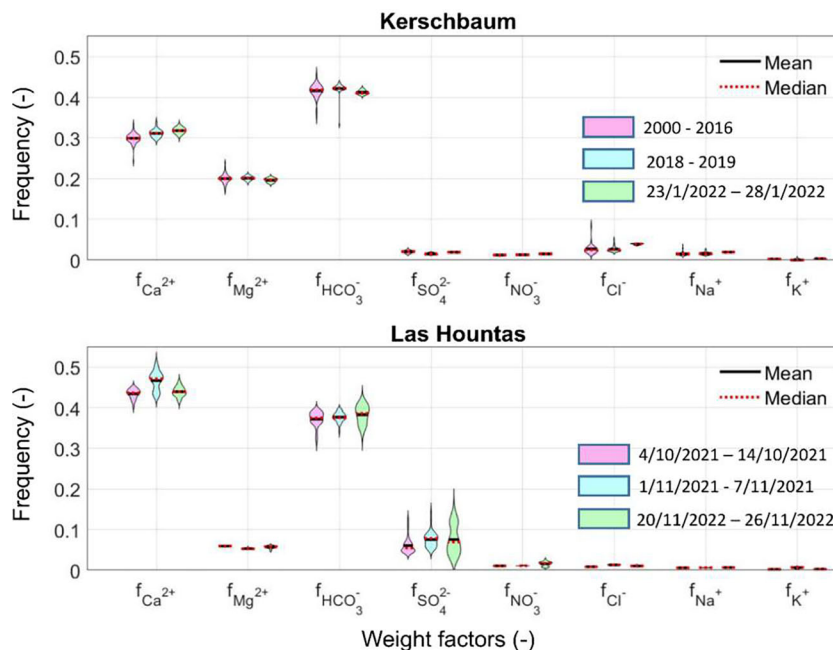


FIGURE 3 Electrical conductivity EC ($\mu\text{S}/\text{cm}$) computed on PHREEQC at the same temporal resolution of the observed water samples given as input, for the Kerschbaum (period 2018–2019) and Las Hountas (event 4/10/2021–14/10/2021) springs. a,b Computed against observed total EC time series, c,d EC relative error (-) time series, e,f charge error (%) time series and g,h probability distribution of the EC relative error (-).

interquartile ranges, with exception of HCO_3 and SO_4 . As shown in Table S1, there is a positive correlation between the relative variation in measured concentrations and relative width of the uncertainty

bands. The method shows low uncertainty in the estimation of Mg and Ca, followed in order by Na, Cl and NO_3 . Whereas, the method is less accurate for HCO_3 and SO_4 , for which it overestimates and

FIGURE 4 Frequency of occurrence of the weight factors f_i of the individual free ions for both the springs and periods. For the Kerschbaum spring, the distributions refer to the periods 2000–2016 (pink), 2018–2019 (blue) and 23/01/2022–28/1/2022 (green); for the Las Hountas spring to the periods 4/10/2021–14/10/2021 (pink), 1/11/2021–7/11/2021 (blue) and 20/11/2022–26/11/2022 (green).



underestimates, respectively, the peak concentrations observed on 4 October 2021 (Figure 5). Finally, the large uncertainty in the estimates for K results from the large relative variation in the measured concentration (Table S1).

Figures S2a and S3a show the same analyses for Kerschbaum for the period 2018–2019 and 23 January 2022–28 January 2022, respectively. The results show that the method provides a better interpolation of the observations than in Las Hountas. Moreover, the results are in line with what observed for Las Hountas spring, confirming that the method is more uncertain for those solute species contributing less to the total EC and with larger relative variability. Due to the lack of samples representing the variability at high flow conditions, the behaviour of the peak in January 2019 has to be interpreted as the probable behaviour considering the available information.

3.4 | Predictive model based on the frequency of occurrence of the weight factors f_i

For most solute species, the use of f_i as a random variable allows us to reproduce quite well the observations when we apply the method for interpolation. Therefore, we test under which circumstances the method can be applied to predict the ion content for periods in which only the EC data are available.

Figure 6 shows the predicted high-resolution concentration time series of major solute species for Las Hountas (1 November 2021–7 November 2021 and 20 November 2022–26 November 2022). The weight factors distribution is taken from the event of October 2021, which we use as calibration event. The accuracy of the prediction is for each solute species correlated with changes in the frequency distribution of the related weight factor f_i . More precisely, the larger the difference between the frequency of occurrence of the weight factor observed in the calibration and validation periods (Figure 4) the lower

the accuracy of the estimations. The performance of the decomposition EC method in predicting solute concentrations is hence significantly different in the two validation periods due to the results described in Section 3.2.

The differences between the frequency of occurrence of the weight factors f_i observed for Las Hountas during the events in October and November 2021 are larger than those observed between October 2021 and November 2022 (Figure 4), leading to a less accurate prediction. This is particularly evident for Ca, Mg, Cl and K, whose predicted uncertainty bands for November 2021 show a shift with respect to the observations (Figure 6, left side). On the contrary, being the frequency of occurrence of the weight factors f_i similar between October 2021 and November 2022, the model well predicts the concentrations of Ca and Mg in November 2022 with most of the observations falling in the 10%–90% percentile range (Figure 6, right side). Regarding HCO_3 and SO_4 , all observations fall in the full range of the predicted uncertainty bands for both the validation periods. However, the model overestimates the concentration of HCO_3 and underestimated the concentration of SO_4 at peak conditions observed on 4 November 2021, and 22 November 2022. The not accurate prediction of NO_3 for November 2022 results from the fact that the distribution used as calibration period (October 2021) is characterized by a narrower variability, more similar to that observed in November 2021. The overestimation in the estimates of Cl and Na for November 2022 is due to a shift in the mean weight factors between the calibration and validation periods.

The same analyses were done for Kerschbaum considering the years 2000–2016 as calibration period. Figures S2b and S3b show the prediction for the period 2018–2019 and 23 January 2022–28 January 2022, respectively. Overall, the prediction of the observed concentrations is accurate although the spring displays a small discharge variability and hence the variability in ion concentration is also small.

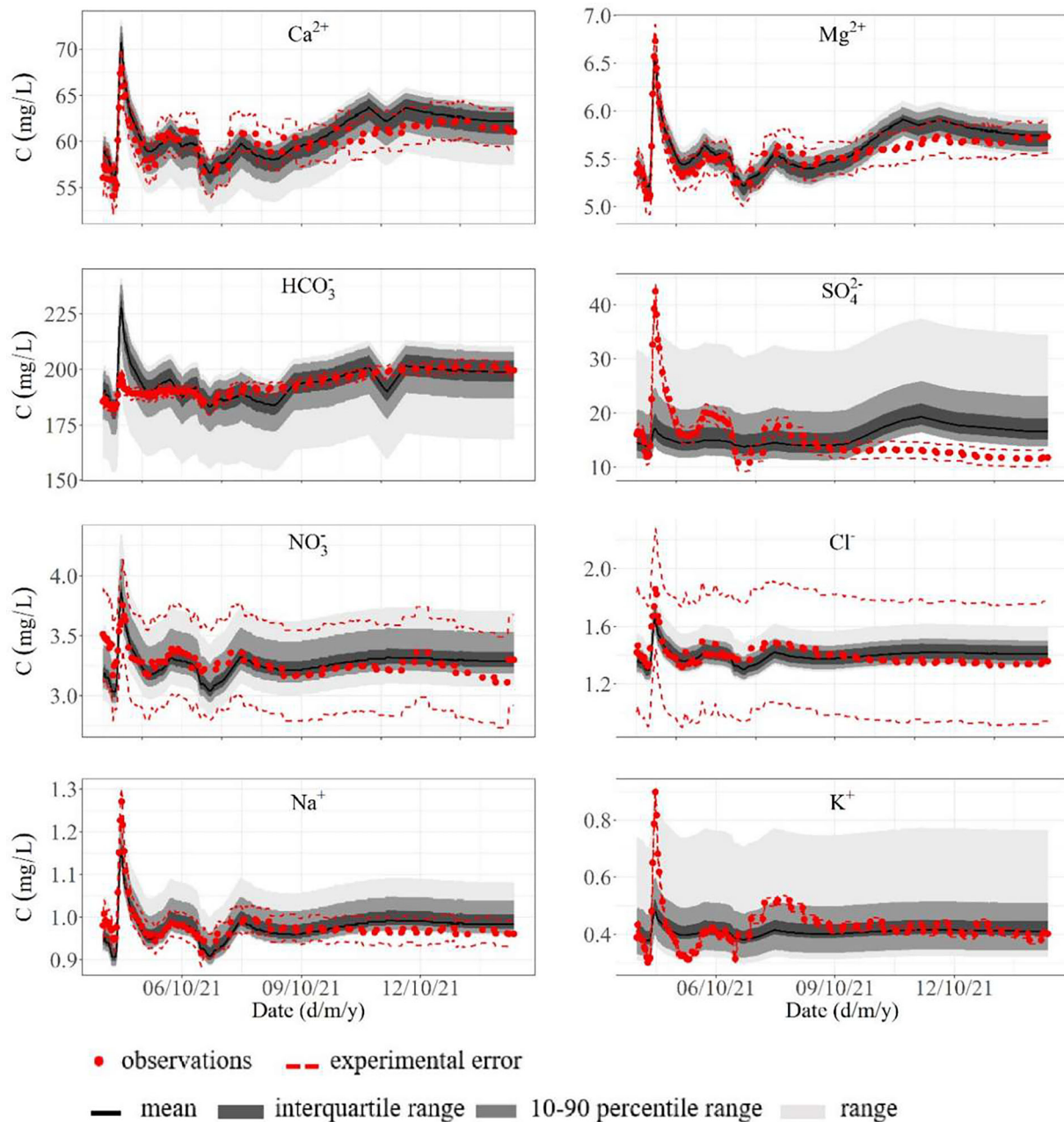


FIGURE 5 Interpolated experimental uncertainty on the individual solute species concentrations (dashed red lines) together with their interpolated uncertainty based on the frequency of occurrence of the observed weight factors (grey bands). The black, grey and light grey areas of the bands represent the interquartile, the 10–90% percentile and full ranges of the computed solute species concentrations (mg/L), respectively. The red points are the observed solute concentrations (mg/L). The concentrations are computed at the Las Hountas spring for the period 4/10/2021–14/10/2021.

4 | DISCUSSION

When comparing the contributions of the solute species present as free ions and as part of complexes to the total concentration, complexation processes are particularly significant for SO_4 , followed in order by Ca, Mg, HCO_3 , and Na (Figure 2a–c). As for the case of SO_4 (Figure 2e,f), for some solute species complexes represent a significant percentage of the total concentration and therefore have a pivotal role when deriving the total solute species concentration from the

measured EC. Being our aim to derive high resolution time series for the solute concentration from the EC measurements, and not vice versa, we can conclude that karst system studies require to account for the role of complexation processes when applying EC decomposition methods to retrieve the concentrations of those solute species which form complexes.

The uncertainty quantification was investigated for both watersheds. Due to the lack of EC and concentration measurements at high flow conditions for Kerschbaum, the analysis of this spring is to some

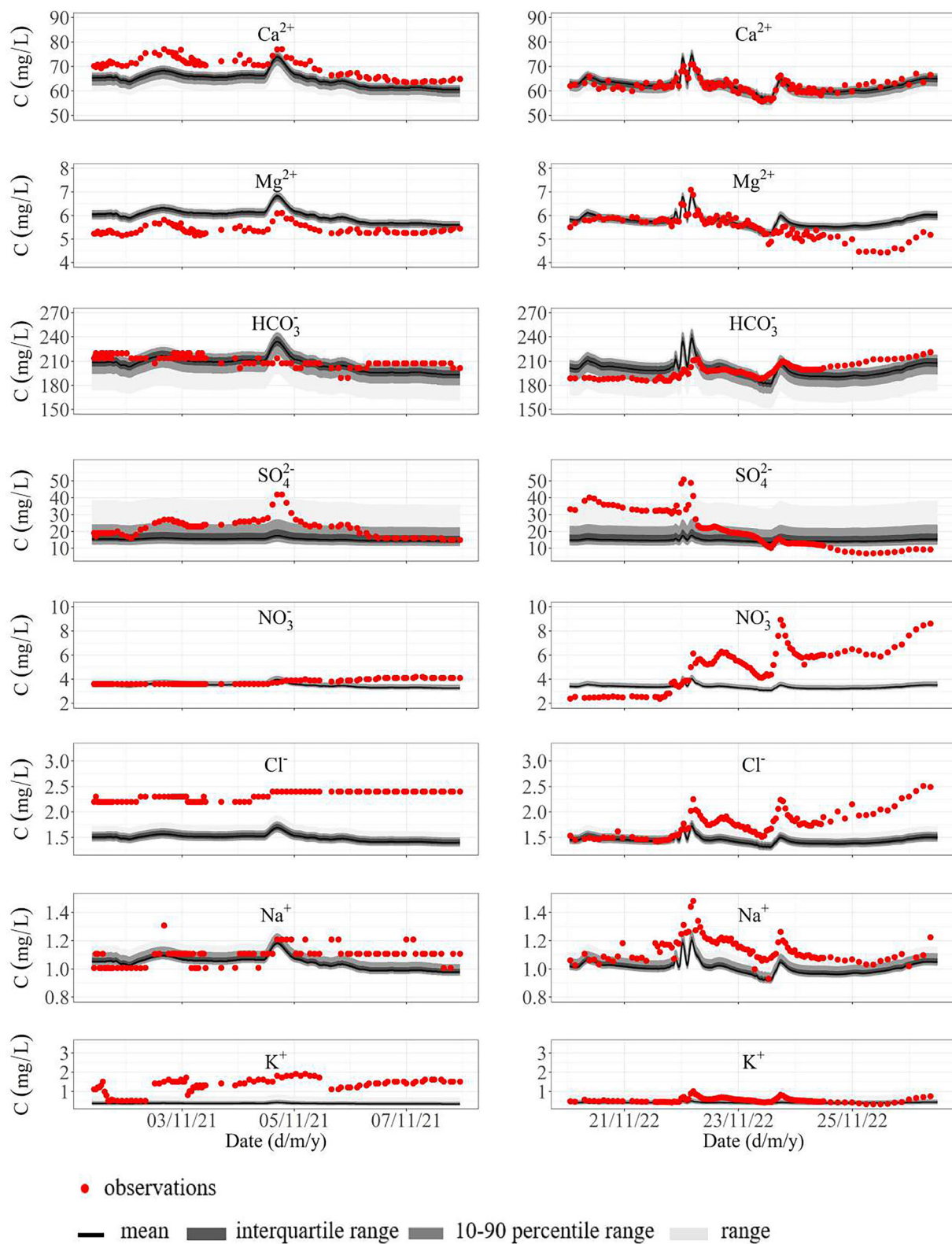


FIGURE 6 Uncertainty bands for the predicted individual solute species (mg/L). The concentrations are computed at the Las Hountas spring for the periods 1/11/2021–7/11/2021 (left side) and for the period 20/11/2022–26/11/2022 (right side) based on the frequency of occurrence of the weight factors observed in 4/10/2021–14/10/2021. The black, grey and light grey areas of the bands represent the interquartile, the 10–90% percentile and full ranges of the computed solute species concentrations (mg/L), respectively. The red points are the observed solute concentrations (mg/L).

extent limited. The inclusion of Kerschbaum in the present work was chosen to investigate the relevance of complexes in karst systems with different geologies. Moreover, the available data show that for catchments with stationary and homogeneous geology the method performs well both for interpolation and prediction purposes.

The results of both the uncertainty quantification during interpolation (Figures 5 and S2a, Table S1) and of the predictive model (Figures 6 and S2b) show a positive correlation between the width of the uncertainty band and the relative variation in concentration. As already observed by Benettin and van Breukelen (2017), the information contained in continuous EC time series better represents the dynamics of those solute species with higher contribution to EC and lower relative variation in concentration. Indeed, due to the use of a linear interpolation for the weight factors f_i , the larger the relative variation of an ion the wider the frequency distribution of its weight factor (Equation 3) and consequently the wider the uncertainty in the computed concentration (Equation 4).

Further interpretations of the results need to consider the different geologies of the study areas, which lead to diverse ion content, temporal variability, and transport processes. Kerschbaum is a dolomitic karst system with a single water contribution to the spring and whose EC comes almost entirely from Ca^{2+} , Mg^{2+} and HCO_3^- (Figure 2b). On the contrary, Baget is a limestone system (lower contribution of Mg^{2+}) characterized by an outcrop impermeable formation of black flysch (Figure 1c), which affects the hydrochemistry of the spring discharge due to pyrite oxidation and thus increasing the

concentration of SO_4^{2-} (Ulloa-Cedamano et al., 2020). The area also includes a gypsum clay formation (Figure 1c), which we do not consider significantly impacting the hydrochemistry of the system due to its minor extension. Due to the black flysch, Baget is not a completely karst system and shows varying contributions of water from different geological formations during different events. This leads to significant changes in the frequency distribution of the weight factors observed between successive events (Figure 4) and consequently affects the performance of the EC decomposition method in both the interpolation and prediction of the individual solutes.

The discharge at Las Hountas shows large variability in solute species concentrations within a precipitation event and between successive events, due to the chemical compositions and response times of the different water contributions. This explains the relevant shifts in the frequency of occurrence of the weight factors f_i observed at the spring between the events in October 2021 and November 2022 on one side and November 2021 on the other (Figure 4). Despite being close in time, the events in October 2021 and November 2021 show different hydrological and geochemical conditions (Figures 7a and S4a) and thus different ion signatures. Consequently, as Figure 6 shows for Ca, Mg and Cl, the dynamic behaviour of the system causes the EC decomposition method to not satisfactorily predict solute species concentrations for November 2021. On the contrary, being the frequency of occurrence of f_i similar between October 2021 and November 2022 (Figure 4), the method well predicts Ca and Mg for November 2022 (Figure 6). The similar frequency of occurrence of the

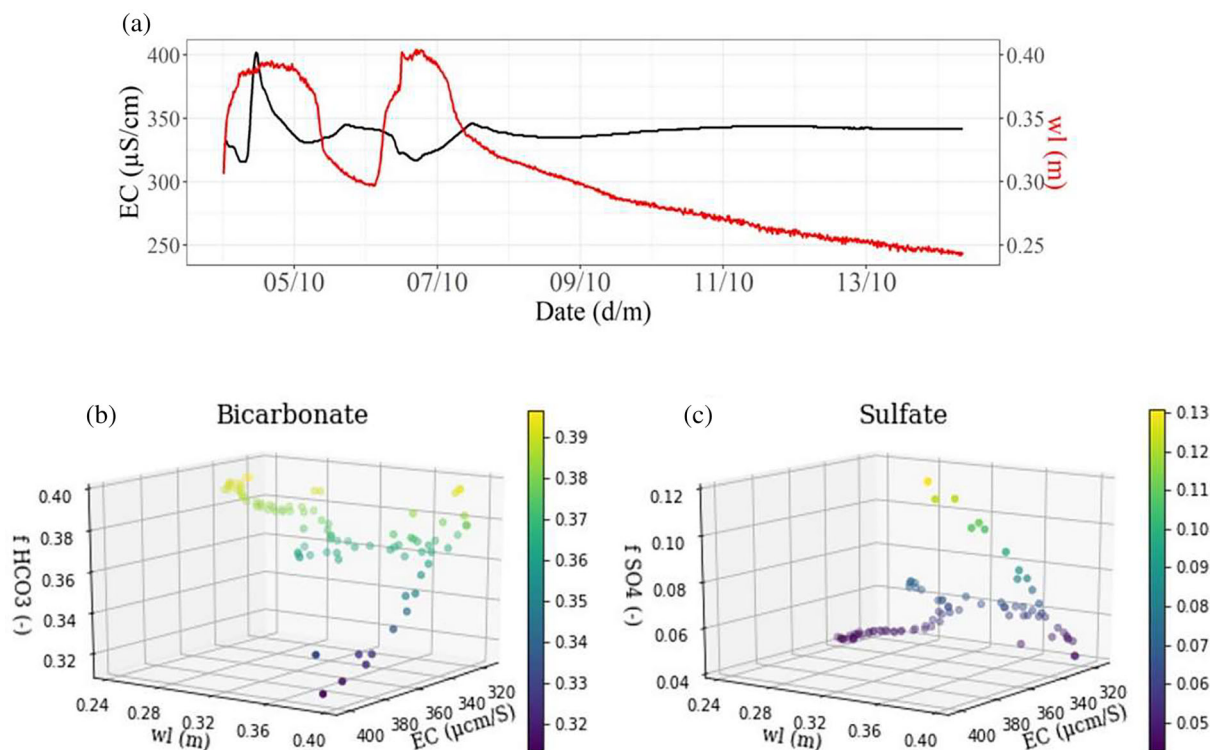


FIGURE 7 Correlation between electrical conductivity EC (μS/cm), water level wl (m) and the weight factors f_i (–) of HCO_3^- and SO_4^{2-} observed at Las Hountas for the period 4/10/2021–14/10/2021. a Time series of EC (black line) and water level (red line). b 3D scatter plots of EC, water level and weight factor of HCO_3^- . c 3D scatter plots of EC, water level and the weight factors of SO_4^{2-} .

weight factors results from the similar response of the system during the events in October 2021 and November 2022, which are characterized by a sharp increase in water level and piston effect (Figures 7a and 55a). This indicates that to sample the variability of the weight factors in catchments with heterogeneous geology, it is necessary to collect multiple events.

Figure S1 shows the dissolution processes characterizing the limestone and black flysch. According to the stoichiometry of the reactions, the dissolution of CaCO_3 by both H_2CO_3 and H_2SO_4 leads to a lower alkalinity than what we would observe in the case of only dissolution by H_2CO_3 . The reduction in alkalinity explains why the method overestimates HCO_3^- and underestimates SO_4^{2-} at flow peak conditions, both when used to interpolate (Figure 5) and predict (Figure 6) the major solute species concentrations. Figure 8 correlates the percentage reduction in alkalinity (Equation 8) with the tendency of the method to overestimate and underestimate HCO_3^- and SO_4^{2-} ,

respectively. The time series of the equivalent ratio SO_4 over HCO_3 follows the same behaviour of the reduction in alkalinity (Figure 8a), proving the correlation between the dissolution of CaCO_3 by H_2SO_4 and the decrease in HCO_3^- . Figure 8b,c shows the concentrations of HCO_3^- and SO_4^{2-} (black lines) obtained by running the model with only few input concentrations (red points) and using the remaining observations to evaluate the results (grey points). The computed concentrations do not represent properly the increase in HCO_3^- and SO_4^{2-} on October 4, if no measured solute concentrations representing the peak condition are given as input. This results from the fact that during flow peak conditions the weight factors of HCO_3^- and SO_4^{2-} are not adequately predicted by the linear interpolation and consequently the model has no information about the increase in the alkalinity reduction and in the equivalent ratio SO_4 over HCO_3 . Thus, the application of the EC decomposition method at peak conditions requires high-resolution ionic measurements or a better method to estimate

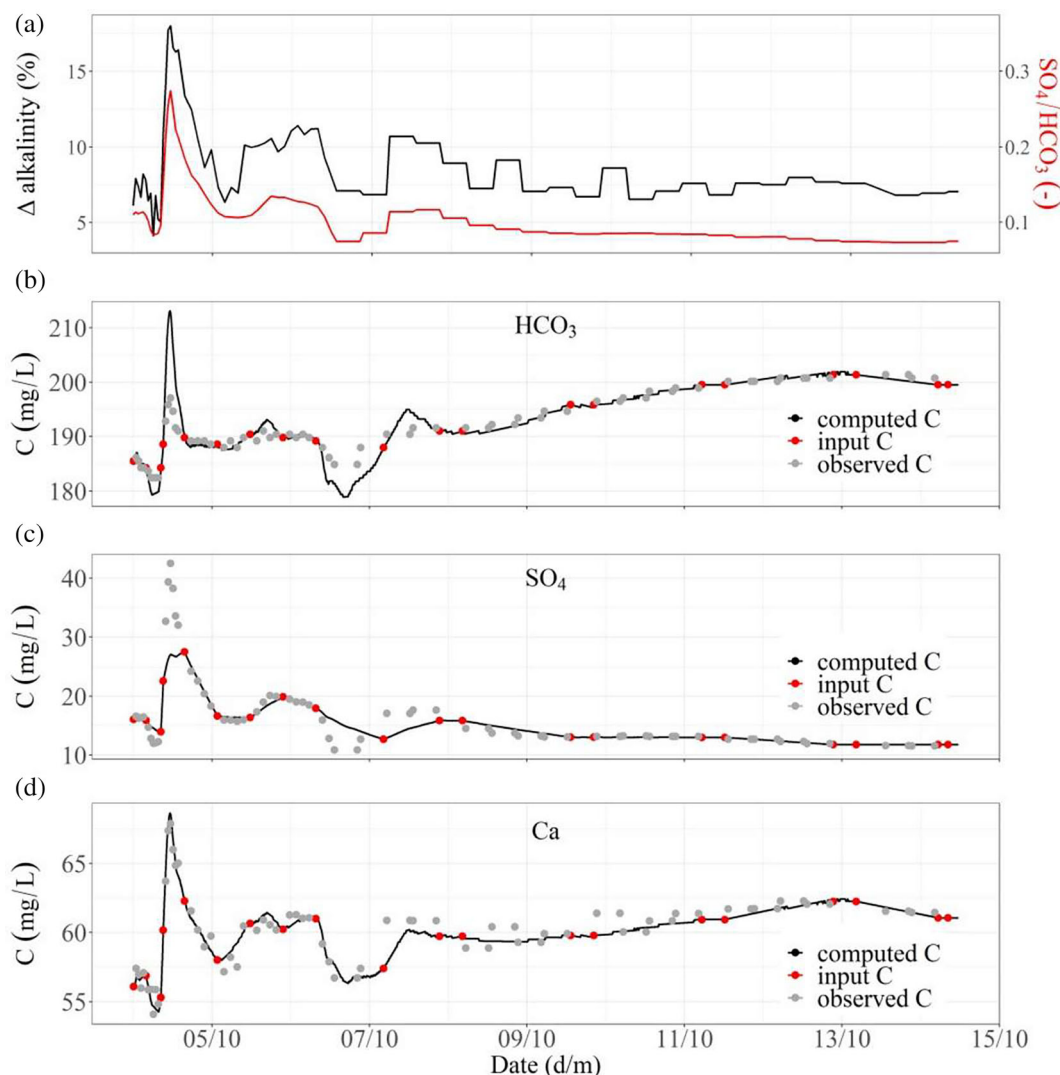


FIGURE 8 Correlation between the reduction in alkalinity due to the carbonate dissolution by sulfuric acid and the model performance (overestimation and underestimation of HCO_3^- and SO_4^{2-} , respectively) at the Las Hountas spring for the event 4/10/2021–14/10/2021. a Time series of the reduction in alkalinity (%) (black line) and the equivalent molar ratio SO_4/HCO_3 (–) (red line). b, c, d Concentrations of HCO_3^- , SO_4^{2-} and Ca (mg/L) obtained by running the model with only few input concentrations (red points).

the weight factors during such conditions. However, the linear interpolation of the weight factors of the other free ions seems to capture the peak conditions. This is the case for Ca (Figure 8d), whose estimated peak concentration well represents the observations.

To investigate the contributions from calcareous rocks and black flysch at different flow conditions, we compare the EC, water level (m) and weight factors f_i of the free ions HCO_3^- and SO_4^{2-} , which were observed at Las Hountas during the event in October 2021 (Figure 7), November 2021 (Figure S4) and November 2022 (Figure S5). As shown in Figure 7a and S5a, the first increase in water level on 4 October 2021, and on 22 November 2022, respectively, is characterized by piston and flushing effects which come with the simultaneous increase in both EC and water level. High values of EC and water levels correspond to low values of $f_{\text{HCO}_3^-}$ and large values of $f_{\text{SO}_4^{2-}}$ (Figures 7b,c and S5b,c). Indeed, during high flow conditions, due to its faster response time, we observe an increase in the relative contribution from the black flysch and a lower relative contribution from the calcareous rocks, which may even be under-estimated due to the existence of surface waters bypassing the spring during flood events (Mangin, 1975; Ulloa-Cedamano et al., 2021). The second rise in water level on 6–7 October 2021, shows dilution processes and thus increase in water level and decrease in EC (Figure 7a). The corresponding increase in $f_{\text{HCO}_3^-}$ and decrease in $f_{\text{SO}_4^{2-}}$ (Figure 7b,c) are explained by the larger contribution of water coming from the karst calcareous formations, which had the time to get activated. Finally, during base flow conditions, the constant EC comes with high values of $f_{\text{HCO}_3^-}$ and low values of $f_{\text{SO}_4^{2-}}$ (Figure 7b,c, Figure S5b,c), indicating that the water mainly comes from calcareous rocks. Therefore, from the comparison of $f_{\text{HCO}_3^-}$ and $f_{\text{SO}_4^{2-}}$ we can understand the dynamics of the system. This allows us to predict when the method is not able to represent the temporal variability in alkalinity reduction. This is the case of 4 October 2021, when the increase in $f_{\text{SO}_4^{2-}}$ (Figure 7c) indicates a larger contribution from the black flysch and a consequent increase in the alkalinity reduction, which is not captured by the method (Figure 8).

5 | SUMMARY

This study investigates how a decomposition of electrical conductivity (EC) signals can be used to retrieve individual solute species concentrations time series in the case of karst systems. Starting from continuous EC and low-frequency water samples, the presented method estimates the concentrations of the major solute species at the same temporal resolution of the observed EC. Due to the large ion content and complex speciation characterizing the discharge of karst springs, it was necessary to compute the distribution of solute species occurring as free ions and as part of aqueous complexes. The concentrations of the free ions, i.e., Ca^{2+} , Mg^{2+} , HCO_3^- , SO_4^{2-} , NO_3^- , Cl^- , Na^+ and K^+ , are derived based on the linear interpolation of the weight factors f_i , which represent the relative contribution of each ion to the total measured EC. Conversely, the concentrations of the solute species involved in complexes are obtained by means of

speciation calculations with PHREEQC as difference between the total molality of a solute (mol/kgw) and the molality of the solution (mol/kgw).

To investigate the relevance of complexation processes, we performed speciation calculations considering two karstic catchments with different geologies and temporal resolution of the available hydrochemical datasets, that is the Kerschbaum dolostone system in Austria and the Baget limestone system in France. The results of the uncertainty quantification performed within this work show that our method can successfully be applied in case of karst systems with a homogeneous geology, as in the case of Kerschbaum. For the latter the EC signal can be used to interpolate and predict with less uncertainty the temporal dynamics of those solute species with large contribution to the total EC and low variability of the weight factor f_i . In case of heterogeneous systems as Baget, the method cannot represent the mixing of the water contributions from the different geological areas of the catchment. The results further show that the correlation between EC, water level and the weight factors of HCO_3^- and SO_4^{2-} can support the investigation of the system functioning, allowing us to distinguish the response of the black flysch formation from that of the calcareous rocks.

The possibility to interpolate high-resolution solute species concentrations time series, without performing continuous—and costly—ionic measurements, has a huge potential in the improvement of hydrochemical data availability and, consequently, supports the understanding of internal transport processes mechanisms and temporal scales.

ACKNOWLEDGEMENTS

This research is part of the ROCKAT project (RObust Conceptualisation of KARst Transport), funded by DFG, CH 981/6-1. The authors further refer to the Interreg Central Europe project boDEREC-CE, funded by ERDF. The water works in Waidhofen a.d. Ybbs provided the orthophoto and the data recorded in the Kerschbaum spring recharge area. Paolo Benettin thanks the ENAC school of the École Polytechnique FÉdÉrale de Lausanne (EPFL) for financial support. On behalf of all authors, the corresponding author states that there is no conflict of interest. Open Access funding enabled and organized by Projekt DEAL.

DATA AVAILABILITY STATEMENT

The data for the Kerschbaum spring for the periods 2000–2016 and 2018–2019 were provided by the waterworks of Waidhofen a.d. Ybbs, whereas the data for the event in January 2022 were collected during an event-based sampling campaign. For the Las Hountas spring the data were collected during the fieldwork in October–November 2021 and in November 2022. The datasets can be downloaded from the Hydroshare repository at the link <http://www.hydroshare.org/resource/fb92daaffced415fb7a991747e73adfa>.

ORCID

Beatrice Richieri  <https://orcid.org/0000-0001-5913-7552>

Paolo Benettin  <https://orcid.org/0000-0001-7556-1417>

REFERENCES

- Aquilina, L., Ladouche, B., & Dörfli, N. (2006). Water storage and transfer in the epikarst of karstic systems during high flow periods. *Journal of Hydrology*, 327(3–4), 472–485. <https://doi.org/10.1016/j.jhydrol.2005.11.054>
- Benettin, P., & Van Breukelen, B. M. (2017). Decomposing the bulk electrical conductivity of streamflow to recover individual solute concentrations at high frequency. *Environmental Science & Technology Letters*, 4(12), 518–522. <https://doi.org/10.1021/acs.estlett.7b00472>
- Bittner, D., Engel, M., Wohlmuth, B., Labat, D., & Chiogna, G. (2021). Temporal scale-dependent sensitivity analysis using discrete wavelet transform and active subspaces. *Water Resources Research*, 57(10), e2020WR028511.
- Bittner, D., Narany, T. S., Kohl, B., Disse, M., & Chiogna, G. (2018). Modeling the hydrological impact of land use change in a dolomite-dominated karst system. *Journal of Hydrology*, 567, 267–279. <https://doi.org/10.1016/j.jhydrol.2018.10.017>
- Cano-Paoli, K., Chiogna, G., & Bellin, A. (2019). Convenient use of electrical conductivity measurements to investigate hydrological processes in alpine headwaters. *Science of the Total Environment*, 685, 37–49. <https://doi.org/10.1016/j.scitotenv.2019.05.166>
- Chang, Y., Hartmann, A., Liu, L., Jiang, G., & Wu, J. (2021). Identifying more realistic model structures by electrical conductivity observations of the karst spring. *Water Resources Research*, 57, e2020WR028587. <https://doi.org/10.1029/2020WR028587>
- Charlier, J. B., Bertrand, C., & Mudry, J. (2012). Conceptual hydrogeological model of flow and transport of dissolved organic carbon in a small Jura karst system. *Journal of Hydrology*, 460, 52–64. <https://doi.org/10.1016/j.jhydrol.2012.06.043>
- Dreiss, S. J. (1989). Regional scale transport in a karst aquifer: 1. Component separation of spring flow hydrographs. *Water Resources Research*, 25(1), 117–125. <https://doi.org/10.1029/wr025i001p00117>
- Fornasini, P. (2008). The uncertainty in physical measurements. In *An Introduction to data analysis in the physics laboratory*. Springer. <https://doi.org/10.1007/978-0-387-78650-6>
- Frank, S., Goepfert, N., Ohmer, M., & Goldscheider, N. (2019). Sulfate variations as a natural tracer for conduit-matrix interaction in a complex karst aquifer. *Hydrological Processes*, 33(9), 1292–1303. <https://doi.org/10.1002/hyp.13400>
- Hacker, P. (2003). *Hydrologisch-hydrogeologische Untersuchungen im Bereich des Glashüttenberges zur Frage des engeren Schutzgebietes für die Kerschbaumer-Quelle*. ARC Seibersdorf research GmbH.
- Hartmann, A., Barberá, J. A., & Andreo, B. (2017). On the value of water quality data and informative flow states in karst modelling. *Hydrology and Earth System Sciences*, 21(12), 5971–5985. <https://doi.org/10.5194/hess-21-5971-2017>
- Hartmann, A., Goldscheider, N., Wagener, T., Lange, J., & Weiler, M. (2014). Karst water resources in a changing world: Review of hydrological modeling approaches. *Reviews of Geophysics*, 52, 218–242. <https://doi.org/10.1002/2013RG000443>
- Hartmann, A., Weiler, M., Wagener, T., Lange, J., Kralik, M., Humer, F., Mizyed, N., Rimmer, A., Barberá, J. A., Andreo, B., Butscher, C., & Huggenberger, P. (2013). Process-based karst modeling to relate hydrodynamic and hydrochemical characteristics to system properties. *Hydrology and Earth System Sciences*, 17(8), 3305–3321. <https://doi.org/10.5194/hess-17-3305-2013>
- Hayashi, M., Vogt, T., Machler, L., & Schirmer, M. (2012). Diurnal fluctuations of electrical conductivity in a pre-alpine river: Effects of photosynthesis and groundwater exchange. *Journal of Hydrology*, 450, 93–104. <https://doi.org/10.1016/j.jhydrol.2012.05.020>
- Hilberg, S., & Schneider, J. F. (2011). The aquifer characteristics of the dolomite formation a new approach for providing drinking water in the northern calcareous Alps region in Germany and Austria. *Water Resources Management*, 25(11), 2705–2729. <https://doi.org/10.1007/s11269-011-9834-x>
- In-Situ Inc. (2012). Aqua TROLL operator's manual: Aqua TROLL 100 – Aqua TROLL 200. https://www.geotechenv.com/Manuals/In-Situ_Manuals/AquaTroll_100-200_Manual.pdf
- Jourde, H., Massei, N., Mazzilli, N., Binet, S., Batiot-Guilhe, C., Labat, D., Steinmann, M., Bailly-Comte, V., Seidel, J. L., Arfib, B., Charlier, J. B., Guinot, V., Jardani, A., Fournier, M., Aliouache, M., Babic, M., Bertrand, C., Brunet, P., Boyer, J. F., ... Wang, X. (2018). SNO KARST: A French network of observatories for the multidisciplinary study of critical zone processes in karst watersheds and aquifers. *Vadose Zone Journal*, 17(1), 1–18. <https://doi.org/10.2136/vzj2018.04.0094>
- Lechuga-Crespo, J. L., Ruiz-Romera, E., Probst, J. L., Unda-Calvo, J., Cuervo-Fuentes, Z. C., & Sánchez-Pérez, J. M. (2020). Combining punctual and high frequency data for the spatiotemporal assessment of main geochemical processes and dissolved exports in an urban river catchment. *Science of the Total Environment*, 727, 138644.
- Liu, Z., Groves, C., Yuan, D., & Meiman, J. (2004). South China karst aquifer storm-scale hydrochemistry. *Ground Water*, 42(4), 491–499. <https://doi.org/10.1111/j.1745-6584.2004.tb02617.x>
- Mangin, A. (1975). Contribution à l'étude hydrodynamique des aquifères karstiques. *Annales de Spéléologie*, 29(3), 283–332 29(4), 495–601; 30(1), 21–124.
- Massei, N., Mahler, B. J., Bakalowicz, M., Fournier, M., & Dupont, J. P. (2007). Quantitative interpretation of specific conductance frequency distributions in karst. *Ground Water*, 45(3), 288–293. <https://doi.org/10.1111/j.1745-6584.2006.00291.x>
- Meus, P., Moureaux, P., Gailliez, S., Flament, J., Delloye, F., & Nix, P. (2014). In situ monitoring of karst springs in Wallonia (southern Belgium). *Environmental Earth Sciences*, 71(2), 533–541. <https://doi.org/10.1007/s12665-013-2760-x>
- Mewes, B., Oppel, H., Marx, V., & Hartmann, A. (2020). Information-based machine learning for tracer signature prediction in karstic environments. *Water Resources Research*, 56, e2018WR024558. <https://doi.org/10.1029/2018WR024558>
- Mudarra, M., & Andreo, B. (2011). Relative importance of the saturated and the unsaturated zones in the hydrogeological functioning of karst aquifers: The case of Alta Cadena (southern Spain). *Journal of Hydrology*, 397(3–4), 263–280. <https://doi.org/10.1016/j.jhydrol.2010.12.005>
- Odeh, T., Salameh, E., Schirmer, M., & Strauch, G. (2009). Structural control of groundwater flow regimes and groundwater chemistry along the lower reaches of the Zerka River, West Jordan, using remote sensing, GIS, and field methods. *Environmental Geology*, 58, 1797–1810. <https://doi.org/10.1007/s00254-008-1678-1>
- Parkhurst, D. L., & Appelo, C. A. J. (2013). *Description of input and examples for PHREEQC version 3-a computer program for speciation, batch-reaction, one-dimensional transport, and inverse geochemical calculations*. U.S. Geological Survey Techniques and Methods, Book 6, Chapter A43 (p. 497). U.S. Geological Survey. <http://pubs.usgs.gov/tm/06/a43>
- Pfaff, J. D. (1993). Method 300.0 – Determination of Inorganic Anions by Ion Chromatography. https://www.epa.gov/sites/default/files/2015-08/documents/method_300-0_rev_2-1_1993.pdf
- Ravbar, N., Engelhardt, I., & Goldscheider, N. (2011). Anomalous behavior of specific electrical conductivity at a karst spring induced by variable catchment boundaries: The case of the Podstenjšek spring, Slovenia. *Hydrological Processes*, 25(13), 2130–2140. <https://doi.org/10.1002/hyp.7966>
- Sheikhy Narany, T., Bittner, D., Disse, M., & Chiogna, G. (2019). Spatial and temporal variability in hydrochemistry of a small-scale dolomite karst environment. *Environmental Earth Sciences*, 78, 273. <https://doi.org/10.1007/s12665-019-8276-2>
- Somridhivej, B., & Boyd, C. E. (2016). An assessment of factors affecting the reliability of total alkalinity measurements. *Aquaculture*, 459, 99–109. <https://doi.org/10.1016/j.aquaculture.2016.03.032>

- Torresan, F., Fabbri, P., Piccinini, L., Dalla Libera, N., Pola, M., & Zampieri, D. (2020). Defining the hydrogeological behavior of karst springs through an integrated analysis: A case study in the Berici Mountains area (Vicenza, NE Italy). *Hydrogeology Journal*, 28, 1229–1247. <https://doi.org/10.1007/s10040-020-02122-0>
- Ulloa-Cedamano, F., Probst, A., Dos-Santos, V., Camboulive, T., Granouillac, F., & Probst, J.-L. (2021). Stream Hydrochemical response to flood events in a multi-lithological karstic catchment from the Pyrenees Mountains (SW France). *Water*, 13(13), 1–25. <https://doi.org/10.3390/w13131818>
- Ulloa-Cedamano, F., Probst, J.-L., Binet, S., Camboulive, T., Payre-Suc, V., Pautot, C., Bakalowicz, M., Beranger, S., & Probst, A. (2020). A forty-year karstic critical zone survey (Baget catchment, Pyrenees-France): Lithologic and hydroclimatic controls on seasonal and inter-annual variations of stream water chemical composition, pCO₂, and carbonate equilibrium. *Water*, 12(5), 1227. <https://doi.org/10.3390/w12051227>

SUPPORTING INFORMATION

Additional supporting information can be found online in the Supporting Information section at the end of this article.

How to cite this article: Richieri, B., Bittner, D., Hartmann, A., Benettin, P., van Breukelen, B. M., Labat, D., & Chiogna, G. (2023). Using continuous electrical conductivity measurements to derive major solute concentrations in karst systems. *Hydrological Processes*, 37(6), e14929. <https://doi.org/10.1002/hyp.14929>